Lab on a Chip

PAPER

View Article Online
View Journal

Cite this: DOI: 10.1039/c5lc00578g

Numerical design and optimization of hydraulic resistance and wall shear stress inside pressure-driven microfluidic networks

Hazem Salim Damiri[a] and Hamzeh Khalid Bardaweel*[ab]

Microfluidic networks represent the milestone of microfluidic devices. Recent advancements in microfluidic technologies mandate complex designs where both hydraulic resistance and pressure drop across the microfluidic network are minimized, while wall shear stress is precisely mapped throughout the network. In this work, a combination of theoretical and modeling techniques is used to construct a microfluidic network that operates under minimum hydraulic resistance and minimum pressure drop while constraining wall shear stress throughout the network. The results show that in order to minimize the hydraulic resistance and pressure drop throughout the network while maintaining constant wall shear stress throughout the network, geometric and shape conditions related to the compactness and aspect ratio of the parent and daughter branches must be followed. Also, results suggest that while a "local" minimum hydraulic resistance can be achieved for a geometry with an arbitrary aspect ratio, a "global" minimum hydraulic resistance occurs only when the aspect ratio of that geometry is set to unity. Thus, it is concluded that square and equilateral triangular cross-sectional area microfluidic networks have the least resistance compared to all rectangular and isosceles triangular cross-sectional microfluidic networks, respectively. Precise control over wall shear stress through the bifurcations of the microfluidic network is demonstrated in this work. Three multi-generation microfluidic network designs are considered. In these three designs, wall shear stress in the microfluidic network is successfully kept constant, increased in the daughter-branch direction, or decreased in the daughter-branch direction, respectively. For the multi-generation microfluidic network with constant wall shear stress, the design guidelines presented in this work result in identical profiles of wall shear stresses not only within a single generation but also through all the generations of the microfluidic network under investigation. The results obtained in this work are consistent with previously reported data and suitable for a wide range of lab-on-chip applications.

Received 25th May 2015,
Accepted 11th August 2015

DOI: 10.1039/c5lc00578g

www.rsc.org/loc

Introduction

Chief among microfluidic developing technologies are bio-microfluidic devices inspired by biological systems found in living organs in nature.[1,2] For example, great efforts have been put forward by several groups to mimic the organs found in mammals such as the kidney[2] and the lung.[1,3] Often, this is referred to as *organ-on-a-chip*. The so-called *organ-on-a-chip* consists of several chambers filled with specified cell cultures and connected through a network of microchannels.[4] Similar to the vessels containing blood in our bodies, these microfluidic channels facilitate the recirculation of the culture medium flowing inside the microfluidic device. Most often, the network consists of several channels bifurcated into two or more branches where the fluids either combine or split into different directions.

The design process of a microfluidic network is a crucial component of any microfluidic device. In their study of microfluidic blood devices, Gilbert, Richards *et al.* pointed out that factors such as large pressure drop and complex microfluidic channel geometries limit their performance.[5] For example, studies have shown that wall shear stress and geometry of bifurcation play a crucial role in the pathogenesis of artery diseases. Also, studies have shown that controlling the shear stress inside the microfluidic network is beneficial.[6] For instance, in some applications, maintaining a low and constant shear stress throughout the microfluidic network is required to prevent damage to cells sensitive to shear stress, and increase their chances of binding to surfaces.[7] On the other hand, gradually increasing the shear stress inside the microfluidic network used in heavily-laden particulate flow is required to prevent blockage in smaller channels.[7] Moreover, high pressure drops and shear stresses inside the

[a] Department of Mechanical Engineering, Faculty of Engineering and Technology, The University of Jordan, Amman, Jordan
[b] Institute for Micromanufacturing, College of Engineering and Science, Louisiana Tech University, Ruston, Louisiana 71272, USA. E-mail: hamzehb@latech.edu

microfluidic network are linked directly to hemolysis and thrombosis.[5] A hemolysis condition is associated with red blood cells rupture and release of hemoglobin from within the red blood cells into the blood plasma stream while thrombosis condition results in blood clot formation.[5] In addition, as pressure drop and flow resistance increase, the power needed to operate the microfluidic device increases.[8] Higher power consumption may cause an increase in the device occupied volume and thus limit its use in several applications. In tissue engineering, there is a growing need for robust microfluidic network circulation systems to effectively distribute nutrients and exchange oxygen.[4] Thus, the effectiveness of the whole microfluidic device is strongly tied to the fluid flow behavior inside the microfluidic network. As a result, prediction of wall shear stress and hydraulic resistance inside the microfluidic network, with high accuracy, is mandated.[9] Although several techniques have been reported in the literature to measure the wall shear stress inside microfluidic devices,[10,11] there is lack of design rules for optimized microfluidic networks which enable precise control over wall shear stress while maintaining uniform flow rate, minimum pressure drop, and minimum flow resistance across the microfluidic network.

One of the first few mathematical modeling works related to microfluidic networks was done by Murray.[12] Murray used the principle of minimum work to derive an optimum relationship between the parent and daughter branches in cardiovascular systems. His derivation led to the well-known Murray's law which states that the cube of the diameter of the parent vessel must be equal the sum of the cubes of the diameters of the daughter vessels in order to minimize the work required to maintain the flow. Here, the parent and daughter vessels refer to the original and branched microfluidic channels containing the flowing fluid. Although Murray's work is considered the most pioneering work related to the design of microfluidic networks, since then, several attempts have been put forward in order to enhance the design process of microfluidic networks. For example, Oh *et al.* investigated the design of pressure-driven microfluidic networks using the analogy between the fluidic system and electrical circuits.[13] In their work, pressure, flow rate, and hydraulic resistance were analogized to voltage, current, and electrical resistance, respectively. Then, an equivalent electrical circuit was built and analyzed. Razavi *et al.* investigated the geometry of microfluidic networks numerically.[14,15] The model used constructal theory to optimize the performance of the network for different design parameters including cross-sectional areas, length of microfluidic channels, and shapes of the cross-section. The results from their model were in good agreement with Murray's law. Minimization of the hydraulic resistance of the microfluidic network led to constant ratios between consecutive cross-sectional areas and lengths. Motivated by the design of surgeries and interventions found in cardiovascular medicine, Marsden *et al.*[16] introduced a computational framework based on a derivative-free approach along with a mesh adaptive direct search method to obtain a local minimum and thus, optimized the design of the microfluidic network. As an example of his computations, Marsden *et al.* used his computational framework to reproduce Murray's problem. Unlike Murray's original work, his computational solution was extended to consider three-dimensional pulsatile solutions of the Navier–Stokes equations and was not restricted to the Poiseuille flow assumption made by Murray. The response to pulsatile flow in the microfluidic network was also considered by Painter *et al.*,[17] Kanaris *et al.*,[18] and Anastasiou *et al.*[19] Moreover, Barber *et al.*[6] investigated the generalization of Murray's law to consider microfluidic networks of constant-depth arbitrary-shaped cross sections such as rectangular and trapezoidal cross-sectional shaped microfluidic networks. In addition, using Murray's law, Zografos *et al.*[20] studied the Newtonian and power-law non-Newtonian fluid flows in a constant-depth rectangular planar microfluidic network using an in-house code to perform computational fluid dynamics simulation. The model measured the shear stress and flow hydraulic resistance inside the microfluidic network. Another attempt to study the behavior of non-Newtonian blood inside a network of microfluidic channels was done by Revellin *et al.*[21] In their work, Revellin *et al.* derived an analytical expression of Murray's law for blood inside a circular cross-section using the power-law model assuming two different constraints in addition to the pumping power. The two constraints were volume constraint and surface constraint. Their results showed that under the volume constraint, classical Murray's principle is valid and the relationship between the parent and daughter vessels is independent of the fluid properties. In contrast, under the surface constraint, different values from Murray's law may be obtained and the relationship between parent and daughters vessels depends on the fluid properties.[21] A simple model for fully developed laminar non-Newtonian fluid flow in a non-circular microfluidic network was investigated by Muzychka *et al.*[22] The model used power-law fluids based on Rabinowitsch–Mooney formulation and was verified for a rectangular cross-sectional area within 10% accuracy. Reis *et al.*[23] used the constructal theory to investigate the flow inside non-symmetric network structures found in human respiratory and circulatory systems. Their results showed that global flow resistances depend on the degree of asymmetry between branches in each bifurcation. Other attempts to investigate the behavior of a microfluidic network include the work done by Shan *et al.*,[24] Hoganson *et al.*,[25] Gat *et al.*,[26] Tondeur *et al.*,[27] and Tonomura *et al.*[28]

Previous discussion reveals the significance of using modeling tools in understanding and improving the design of microfluidic networks widely present in microfluidic devices. The goal of the work presented in this article is to offer general guidelines for the design and optimization processes of different cross-sectional shapes and geometries of microfluidic networks. In this work, wall shear stress and hydraulic resistance inside the microfluidic network are linked directly to design parameters such as cross-sectional area and perimeter of the geometry under investigation. The

distribution of wall shear stress inside the bifurcated branches of the microfluidic network is investigated thoroughly, and techniques for controlling shear stress inside each microfluidic branch are provided. Similarly, minimization of hydraulic resistance throughout the network is investigated and related to the microfluidic network geometry and shape. Work is carried out using a combination of multiphysics finite element COMSOL modeling and analytical techniques. The constraints used in this work are constant fluid volume flowing through the network, constant volume of the network, and constant material surface area. On the one hand, a constant volume flow rate constraint is drawn from the need to deliver the same amount of fluid to the designated point all the time. On the other hand, optimizing the microfluidic network requires the use of a fixed surface area and minimum material upon designing the microfluidic network.

Theory

In this section, the behavior of the microfluidic network is formulated. This is done by formulating the effects of geometries and dimensions on minimizing hydraulic resistances and controlling shear stresses throughout microfluidic networks. Fig. 1 shows an example of a microfluidic network used in microfluidic devices. The Navier–Stokes equation is used to describe the continuous flow behavior inside the microfluidic network, given by

$$\rho\frac{\partial v}{\partial t}+\rho v\cdot\nabla v=-\nabla p+\nabla\cdot\tau \tag{1}$$

For a fully developed, steady, laminar, and pressure-driven flow inside an arbitrary-shaped constant cross-sectional area network, shown in Fig. 2, summation of forces on the channel boundaries leads to:

$$Ap_{\text{in}}-Ap_{\text{out}}-\bar{\tau}PL=0. \tag{2}$$

Further, pressure drop ΔP and hydraulic resistance R are related through:

$$\Delta p=RQ, \tag{3}$$

where Q is the volume flow rate ($m^3\ s^{-1}$), and R is the hydraulic resistance for an arbitrary shaped geometry, shown in Fig. 2 and given by

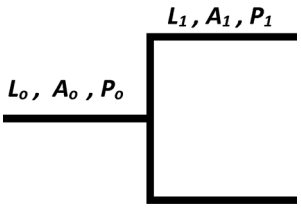

Fig. 1 Example of microfluidic network used in microfluidic devices.

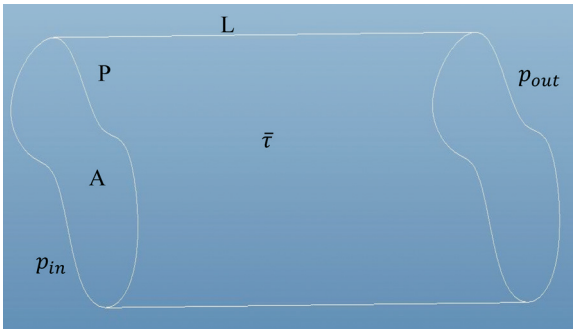

Fig. 2 Arbitrary shaped constant cross-sectional area microfluidic channel.

$$R=\frac{\mu L\beta}{A^2}. \tag{4}$$

Here, the coefficient β is the geometric factor that is a linear function of compactness, *i.e.* C,[29] given by:

$$\beta=Ca+b, \tag{5}$$

where $C=\frac{P^2}{A}$ and a & b are two constants that depend on the shape of the cross-sectional area of the microfluidic channel. For example, for a rectangular cross-sectional area, the geometric factor β is given by:[29]

$$\beta=\frac{22}{7}C-\frac{65}{3}. \tag{6}$$

Using the set (eqn (2)–(4)), the average wall shear stress $\bar{\tau}$ can be rewritten as:

$$\bar{\tau}=\beta\frac{\mu U}{P}. \tag{7}$$

For a bifurcating network, shown in Fig. 1, with an arbitrary cross-sectional shape, shown in Fig. 2, a constant wall shear stress requirement between the parent ($\bar{\tau}_o$) and the daughter ($\bar{\tau}_1$) channels yields:

$$\beta_o\frac{\mu U_o}{P_o}=\beta_1\frac{\mu U_1}{P_1} \tag{8}$$

Applying the continuity equation over a control volume of the microfluidic network gives:

$$\frac{U_1}{U_0}=2^{-1}\frac{A_0}{A_1}. \tag{9}$$

Substituting the continuity equation (eqn (9)) and the geometric factor β (eqn (5)) into eqn (8) yields:

$$\left(\frac{P_0}{A_0^{\,2}}a+\frac{b}{A_0P_0}\right)=\left(\frac{P_1}{2A_1^{\,2}}a+\frac{b}{2A_1P_1}\right) \tag{10}$$

Equating the coefficients on both sides of eqn (10) yields:

$$A_0 = 2^{\frac{2}{3}} A_1. \tag{11a}$$

$$P_0 = 2^{\frac{1}{3}} P_1. \tag{12a}$$

Here, the area-bifurcation ratio given in eqn (11a) is consistent with the previous work reported by Razavi *et al.*[14] This is also in agreement with Murray's original work which stated that the cube of the diameter of a circular parent vessel D_o must be equal the sum of the cubes of the diameters of the daughter vessels D_1 in order to minimize the work required to maintain the flow. The previous derivation can be easily extended to a multi-generation microfluidic network. For consecutive generation inside the microfluidic network, a branching parameter, X, is introduced.[6,20,30] The branching parameter X is defined in terms of the ratio of the consecutive generation diameters, *i.e.* $X = \frac{1}{2}\left(\frac{D_i^3}{D_{i+1}^3}\right)$ Thus, for a multi-generation network, the set (eqn (11a) & (12a)) is extended to:

$$A_0 = 2^{\frac{2n}{3}} X^{\frac{2n}{3}} A_n. \tag{11b}$$

$$P_0 = 2^{\frac{n}{3}} X^{\frac{n}{3}} P_n. \tag{12b}$$

To investigate the effect of bifurcation ratios appearing in set (eqn (11b) and (12b)), the area and perimeter power coefficients in eqn (11b) & (12b) are replaced with a generalized area power coefficient $(1/\alpha_1)$ and a generalized perimeter power coefficient $(1/\alpha_2)$, respectively, yielding:

$$A_0 = 2^{\frac{2n}{\alpha 1}} X^{\frac{2n}{\alpha 1}} A_n. \tag{13}$$

$$P_0 = 2^{\frac{n}{\alpha 2}} X^{\frac{n}{\alpha 2}} P_n. \tag{14}$$

Subjecting the microfluidic network design to constant volume $V_{constant}$ and constant surface area $SA_{constant}$ constraints yields:

$$L_i A_i + 2L_{i+1}A_{i+1} = V_{constant} \tag{15}$$

$$L_i P_i + 2L_{i+1}P_{i+1} = SA_{constant} \tag{16}$$

For given lengths of the microfluidic network and specified power coefficients, *i.e.* α_1 and α_2 the set (eqn (13)–(16)) is solved to find the geometry of the parent and daughter branches. For example, a single generation network with a rectangular cross-sectional area is considered (Fig. 1). Given, L_o, L_1, α_1 and α_2 the set (eqn (13)–(16)) can be used to determine the widths and depths of the parent and daughter branches of the microfluidic network, *i.e.* ω_0, D_0, ω_1, and D_1, respectively. Then, the total hydraulic resistance for the bifurcating network is given by:

$$R_{total} = \frac{\mu L_0 \beta_0}{A_0^2} + \frac{\mu L_1 \beta_1}{2A_1^2}, \tag{17}$$

where $A_0 = d_0\omega_0$ & $A_1 = d_1\omega_1$ calculated using eqn ((13)–(16)) and the geometric factor β is calculated using eqn (6). The average wall shear stresses $\bar{\tau}$ in parent and daughter branches are given by eqn (7), *i.e.* $\bar{\tau}_0 = \beta_0 \frac{\mu U_0}{P_0}$ and $\bar{\tau}_1 = \beta_1 \frac{\mu U_1}{P_1}$, respectively, and the perimeters are $P_0 = 2(d_0 + \omega_0)$ & $P_1 = 2(d_1 + \omega_1)$.

Further, equating the coefficients in eqn (10) and dividing the two resultant equations yield:

$$\frac{P_0^2}{A_0} = \frac{P_1^2}{A_1} = C. \tag{18}$$

Thus, an optimum design of the microfluidic network requires a fixed compactness C of the parent and daughter branches, *i.e.* $C_o = C_1$. For a circular cross-sectional microfluidic network, the compactness of the network is always constant, *i.e.* $C_o = C_1 = 4\pi$. However, for a rectangular cross-sectional microfluidic network the compactness of the network is dependent on the aspect ratio of the branches. Taking the square root of eqn (18) yields:

$$\frac{P_0}{\sqrt{A_0}} = \frac{P_1}{\sqrt{A_1}}. \tag{19}$$

The ratio in eqn (19), *i.e.* $\frac{P}{\sqrt{A}}$ is a non-dimensional geometrical factor[22,31] that is related to the aspect ratio of the cross-section. For a rectangular cross-sectional microfluidic network, the factor $\frac{P}{\sqrt{A}}$ is related to the aspect ratio by

$$\frac{P}{\sqrt{A}} = \frac{2\left(1 + \left(\frac{1}{\varepsilon}\right)\right)}{\sqrt{1/\varepsilon}}, \tag{20}$$

where ε is the aspect ratio of the branch, *i.e.* $\varepsilon = \frac{\omega}{d}$ The set (eqn (18) & (20)) indicates that for an optimal network design, the aspect ratio should be fixed throughout the network. Thus, to determine the compactness C and the aspect ratio ε that correspond to minimum hydraulic resistance, sets (eqn (11b), (15), (18)) and (eqn (11b), (15), (19), (20)) are solved, respectively. The compactness C obtained is then substituted into eqn (6) and (17) to calculate the hydraulic resistance.

A similar argument can be used for different cross-sectional shapes found in microfabrication. For example, akin to the procedure described above, one can obtain the optimal design of a triangular cross-sectional area microfluidic

network. For instance, the compactness of an isosceles triangular cross-sectional area microfluidic network is given by:

$$C = \frac{\left((2\times l) + B\right)^2}{\frac{1}{2}B^2\sqrt{\frac{l^2}{B^2} - \frac{1}{4}}}, \quad (21)$$

where l is one of the two equal sides (leg length) and B is the base of the triangle. To find the optimum C of the network, eqn (21) is solved for parent and daughter branches along with the set (eqn (11b) and (15)). Hydraulic resistance is then obtained using eqn (17) , where the geometric factor β is given by:[29]

$$\beta = \frac{25}{17}C + \frac{40\sqrt{3}}{17}. \quad (22)$$

Results and discussion

To investigate the performance of various microfluidic networks, the multi-physics modeling software COMSOL is used to run the simulation. Since the Navier–Stokes equation is valid for a continuous fluid, first the continuum assumption is verified for the microfluidic network by calculating the Knudsen number, k_n. For a 1 μm characteristic length and using liquid water as the working fluid, the estimated Knudsen number is $k_n = 3 \times 10^{-4}$ which is smaller than the critical value for the continuum assumption, *i.e.* 1×10^{-3}.[32] For the geometry considered in this article, the smallest characteristic length is larger than 1 μm and thus the continuous flow assumption is valid.

First, a single-generation microfluidic network is investigated. Table 1 lists the geometric parameters and flow conditions used in simulation. Fig. 3–5 show the model and analytical results of flow inside a rectangular cross-sectional area, T-shaped, single generation microfluidic network. Both hydraulic resistance R and wall shear stress ratio $\frac{\bar{\tau}_{inlet}}{\bar{\tau}_{outlet}}$ across the microfluidic network *versus* area power coefficient, α_1, are shown. In Fig. 3–5, the perimeter power coefficients α_2 are held constant, *i.e.* $\alpha_2 = 2$, 3, and 4.5, respectively. For both wall shear stress and hydraulic resistance, the figures reveal good agreement between the model simulation and analytical results obtained using eqn (7) and (17), respectively. Discrepancies between the model simulation and analytical results are possibly attributed to the irregularities in the flow field near the inlet of bifurcations accounted for in simulation. Nonetheless, for small Reynold numbers, pressure losses around junctions and corners can be neglected for calculating hydraulic resistances. Nonetheless, the maximum error in modeled hydraulic resistances is 1.00%, 1.35%, and 1.6%, respectively. While the error is very small, the Y-axis scale is magnified in the figures to show the points of minimum hydraulic resistances. A similar behavior is observed for pressure drop and power loss throughout the microfluidic network.

Table 1 Single-generation microfluidic network simulation parameters

Software and solver	
Software	Comsol Multiphysics 4.4
Geometry software	Solid Works 2014
Supplementary software	Matlab R2013a
Physics type (In Comsol)	Laminar flow
Simulation type (transient or steady)	Steady (stationary solver)
Main solver (coupled or segregated)	Fully coupled
Linear solver (direct or iterative)	Iterative
Geometry	
Network inlet length (n = 0)	4 mm
Single-generation length (n = 1)	4 mm
Network total volume ($V_{constant}$)	3×10^{-10} m^3
Network total surface area ($SA_{constant}$)	8×10^{-6} m^2
Mesh	
Number of elements	(600 000–1000 000)
Element type	Tetrahedral and prism element type
Flow properties	
Material	Water
Viscosity	0.001 Pa s
Density	1000 kg m^{-3}
Reynolds number	2.4142–2.8383
Boundary conditions	
Inlet condition	Constant flow rate (5×10^{-10} m^3 s^{-1})
Outlet condition	Constant pressure (0 Pa, gauge)
Walls	No slip condition

The figures also reveal the behavior of hydraulic resistance and wall shear stress. On the one hand, for a fixed perimeter power coefficient α_2, as the area power coefficient α_1

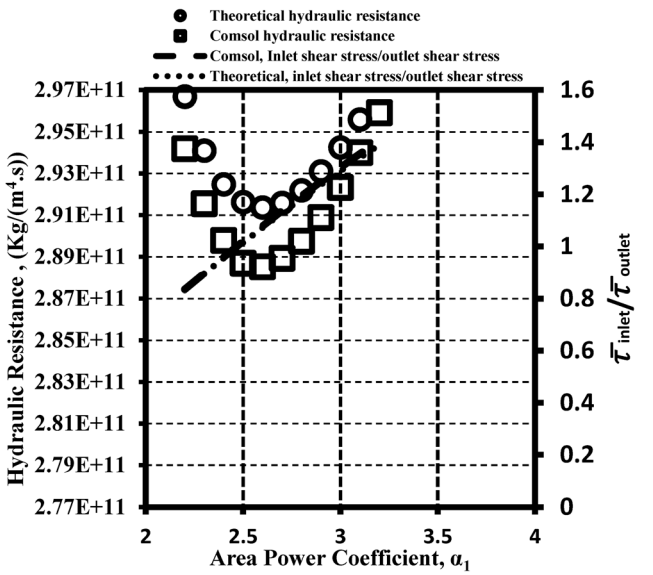

Fig. 3 Model and analytical results of wall shear stress and hydraulic resistance of a single-generation rectangular cross-sectional area, T-shaped, microfluidic network. Perimeter power coefficient, α_2 = 2.

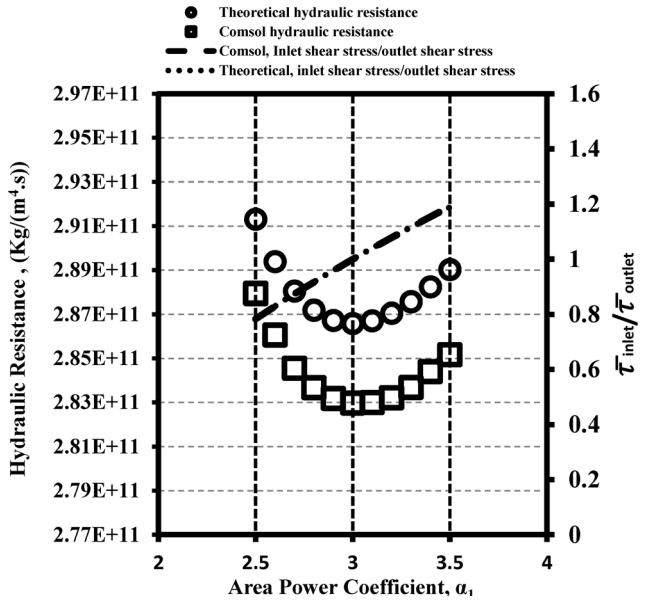

Fig. 4 Model and analytical results of wall shear-stress and hydraulic resistance of a single-generation rectangular cross-sectional area, T-shaped, microfluidic network. Perimeter power coefficient, α_2 = 3.

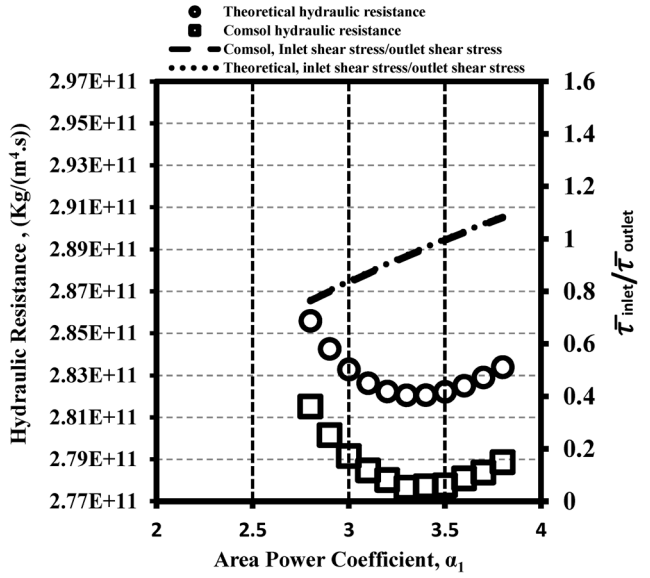

Fig. 5 Model and analytical results of wall shear-stress and hydraulic resistance of a single-generation rectangular cross-sectional area, T-shaped, microfluidic network. Perimeter power coefficient, α_2 = 4.5.

increases, the flow resistance declines to a minimum point and then increases again. On the other hand, the figures also suggest that increasing the perimeter power coefficient α_2, while fixing the area power coefficient α_1 will reduce the minimum hydraulic resistance R_{min} further. That is, for the three perimeter power coefficient cases considered here, *i.e.* α_2 = 2, 3, and 4.5, the minimum hydraulic resistances are R_{min} = 2.9136×10^{11} kg m^{-4} s^{-1} (at α_1 = 2.6, ε_0 = 2.5852, ε_1 = 1.6197), 2.865×10^{11} kg m^{-4} s^{-1} (at α_1 = 3.0, ε_0 = 2.0012, ε_1 = 2.0012), and 2.820×10^{11} kg m^{-4} s^{-1} (at α_1 = 3.3, ε_0 = 1.5362, ε_1 = 2.2364), respectively. Thus, the larger perimeter power coefficients α_2 caused the hydraulic resistance curves shown in Fig. 3–5 to shift further down. However, the wall shear stress ratio $\frac{\bar{\tau}_{inlet}}{\bar{\tau}_{outlet}}$ increases continuously as the area power coefficient α_1 increases. Thus, one can notice that to simultaneously achieve a minimum "local" hydraulic resistance, *i.e.* $R = R_{min}$, and a constant wall shear stress throughout the microfluidic network, *i.e.* $\frac{\bar{\tau}_{inlet}}{\bar{\tau}_{outlet}} = 1$, both area power coefficient and perimeter power coefficient must be equal to 3, *i.e.* $\alpha_1 = \alpha_2 = 3$. It is also worth mentioning that for this optimal case, *i.e.* $\alpha_1 = \alpha_2 = 3$, the aspect ratios of the parent and daughter branches are constant, *i.e.* $\varepsilon_0 = \varepsilon_1 = 2.0012$.

Fig. 6 reveals the effect of width ω to depth d aspect ratio, *i.e.* $\varepsilon = \frac{\omega}{d}$ on the performance of a rectangular cross-section microfluidic network. Here, both area power coefficient and perimeter power coefficient are set to optimum, *i.e.* $\alpha_1 = \alpha_2 = 3$. Fig. 6 reveals that each aspect ratio, $\varepsilon = \frac{\omega}{d}$ will have a minimum "local" hydraulic resistance when $\alpha_1 = \alpha_2 = 3$. Nonetheless, a "global" minimum hydraulic resistance occurs only when the aspect ratio is set to unity, *i.e.* $\varepsilon = 1$ (where the corresponding optimum compactness C is 16). This is also evident in the theoretical results shown in Fig. 6 and obtained by solving the set (eqn (11b), (15), (19) and (20)). Good agreement between modeled and theoretical results is apparent. Thus, a square cross-sectional shaped microfluidic network is the optimal design among all rectangular cross-sectional microfluidic networks. Similarly, by solving the set (eqn (11b), (15) and (21)) for a isosceles triangular cross-sectional area microfluidic network, the results reveal that "global" minimum hydraulic resistance occurs at compactness C = 21 which is close to the compactness of an equilateral (regular isosceles) triangular cross-sectional area, *i.e.* C = 20.7846. Like the square cross-sectional area, all sides and angles are equal in the equilateral triangular cross-sectional area. This suggests that the optimal design of any shape is the regular

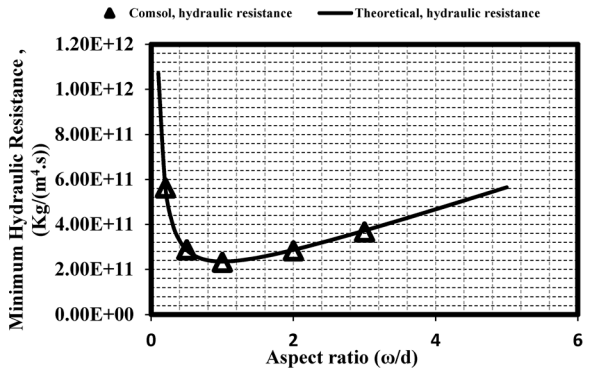

Fig. 6 Effect of aspect ratio ε on the performance of rectangular cross-sectional area microfluidic network.

case. Furthermore, calculating the hydraulic resistances for isosceles triangular, circular, and rectangular cross-sectional area microfluidic networks (for the same flow conditions and optimal configurations) yields $R = 6.4902 \times 10^{11}$ kg m^{-4} s^{-1}, 2.06×10^{11} kg m^{-4} s^{-1}, and 2.35×10^{11} kg m^{-4} s^{-1}, respectively. Thus, for the same conditions, a microfluidic network with a circular cross-sectional area performs better compared to rectangular and isosceles triangular cross-sectional area microfluidic networks.

Fig. 7–9 show the multi-generation microfluidic network behavior for branching parameter, X = 0.7, 1.0, and 1.5, respectively. Table 2 lists all parameters used in multi-generation microfluidic network simulation. Here, both optimum area power coefficient and perimeter power coefficient are used, *i.e.* $\alpha_1 = \alpha_2 = 3$. Fig. 7–9 demonstrate the successful design of microfluidic networks with precise control over wall shear stress from one generation to another. Fig. 7 shows gradually decreasing wall shear stress along the microfluidic network. Fig. 7a shows the modeled and analytical wall shear stress in n-generation, the average $\bar{\tau}_n$ normalized against the average wall shear stress at the inlet of the microfluidic network, $\bar{\tau}_{o,inlet}$. The figure reveals that the average wall shear stress is steadily lowered in the microfluidic network from the wall shear-stress ratio, $\frac{\bar{\tau}_n}{\bar{\tau}_{o,inlet}} = 1$ for n = 0 to the wall shear-stress ratio, $\frac{\bar{\tau}_n}{\bar{\tau}_{o,inlet}} = 0.34$ for n = 3. This is also evident in Fig. 7b which shows the COMSOL simulated wall shear stress in the microfluidic network. Similarly, Fig. 8 presents a

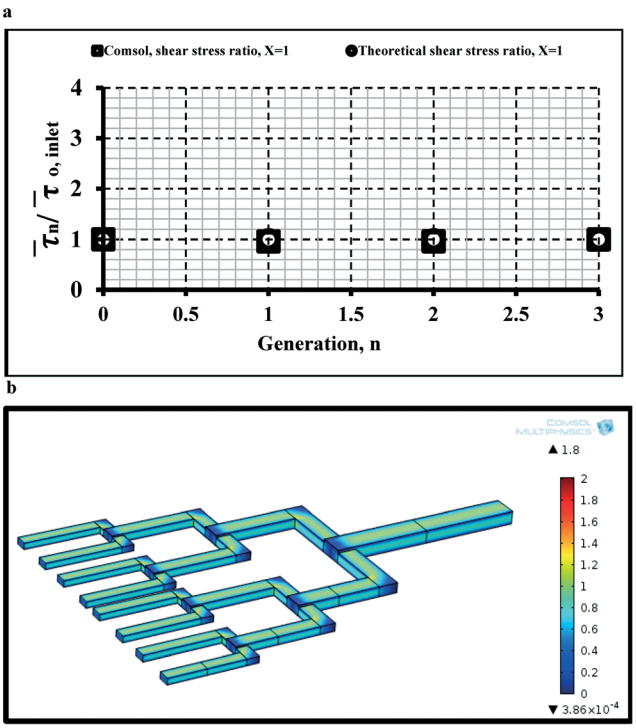

Fig. 8 Mutli-generation microfluidic network, X = 1.0. Control of total wall shear stress in n-generation with respect to inlet wall shear stress (a). COMSOL generated wall shear stress distribution in n-generation (b).

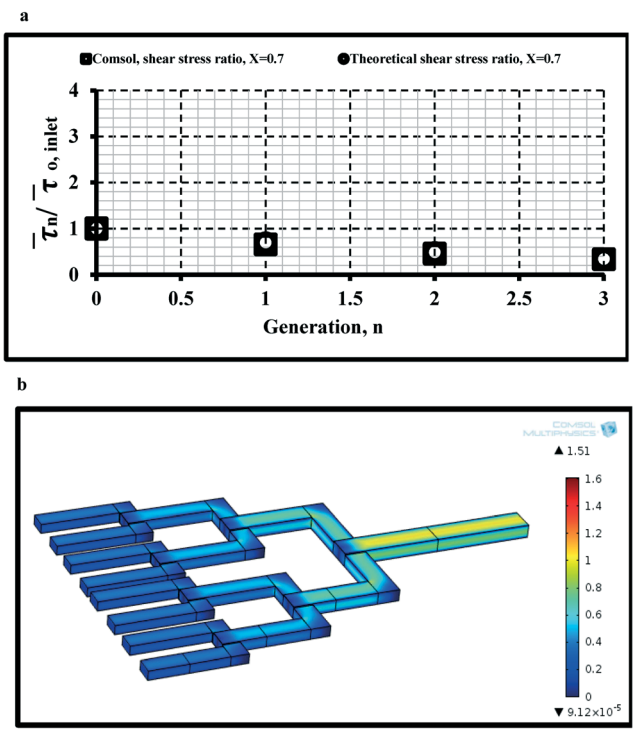

Fig. 7 Mutli-generation microfluidic network, X = 0.7. Control of total wall shear stress in n-generation with respect to inlet wall shear stress (a). COMSOL generated wall shear stress distribution in n-generation (b).

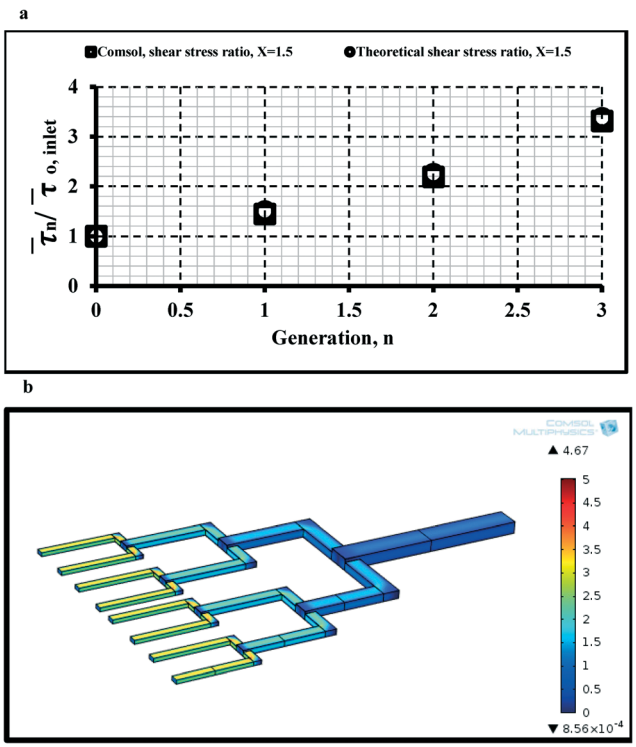

Fig. 9 Mutli-generation microfluidic network, X = 1.5. Control of total wall shear stress in n-generation with respect to inlet wall shear stress (a). COMSOL generated wall shear stress distribution in n-generation (b).

Table 2 Multi-generation microfluidic network simulation parameters

Software and solver	
Software	Comsol Multiphysics 4.4
Geometry software	Solid Works 2014
Supplementary	Matlab R2013a
Physics type (In Comsol)	Laminar flow
Simulation type (transient or steady)	Steady (stationary solver)
Main solver (coupled or segregated)	Fully coupled
Linear solver (direct or iterative)	Iterative
Geometry	
Network inlet width, ω_o	0.25 mm
Network inlet depth, D_o	0.125 mm
Aspect ratio ε (constant throughout the network)	2
Network inlet length, L_o	2 mm
Consecutive length, L_{i+1}	$L_{i+1} = \frac{L_i}{2^{1/3}}$ [14]
Mesh	
Number of elements	(1200 000–2200 000)
Element type	Tetrahedral and prism element type
Simulation parameters	
Material	Water
Viscosity	0.001 Pa s
Density	1000 kg m^{-3}
Reynolds number	2.67
Boundary conditions	
Inlet condition	Constant flow rate (5×10^{-10} m^3 s^{-1})
Outlet condition	Constant pressure (0 Pa, gauge)
Walls	No slip condition

multi-generation microfluidic network design with branching parameter X = 1 suitable for application where a constant wall shear stress is required throughout the network. Here, the average wall shear stress is maintained constant throughout the microfluidic network, *i.e.* $\frac{\overline{\tau}_n}{\overline{\tau}_{o,inlet}} = 1$ Lastly, for applications where the wall shear stress needs to steadily be increased, Fig. 9 shows the case. Here, the average wall shear stress is gradually increased in the microfluidic network from the wall shear stress ratio, $\frac{\overline{\tau}_n}{\overline{\tau}_{o,inlet}} = 1$ for n = 0 to the wall shear stress ratio, $\frac{\overline{\tau}_n}{\overline{\tau}_{o,inlet}} = 3.37$ for n = 3. Results from COMSOL simulation are in good agreement with theoretical results obtained using eqn (7). A similar behavior was reported in the literature.[6]

Fig. 10 shows the normalized wall shear stress distribution in each generation n of the multi-generation microfluidic network for the branching parameter X = 1 obtained using our work (Fig. 10a) and the theory reported in ref. 6 and 30 (Fig. 10b). In Fig. 10a, the wall shear stress distribution in each generation of the rectangular cross-section multi-depth

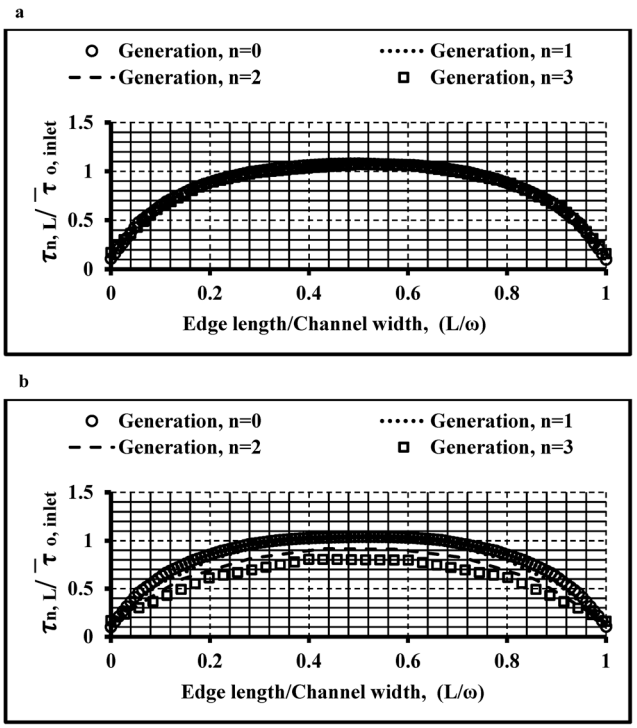

Fig. 10 Normalized wall shear stress distributions calculated using Comsol along the middle upper edge in each generation, n at X = 1. Wall shear stress is normalized against the average shear stress in the inlet channel, n = 0. The edge length is normalized against the channel width in each generation. a) This work and b) using the theory reported in ref. 6 and 30.

network reported in this work is normalized against the mean wall shear stress at the inlet channel, n = 0. Fig. 10b shows the normalized wall shear stress distribution for a rectangular constant-depth multi-generation network reported in ref. 6 and 30. The superiority of the design reported in this work is evident in Fig. 10. That is, Fig. 10a shows that the profiles of wall shear stresses are successfully maintained identical throughout all the generations of the multi-depth microfluidic network. This is presumably because the compactness and thus the aspect ratio are maintained the same in our multi-depth microfluidic network design. This fixed compactness and aspect ratio is achieved by allowing the depth of each generation in the microfluidic network to change along with the width. Nonetheless, the profiles of wall shear stresses shifted to a lower value from one generation to another in Fig. 10b where rectangular constant-depth generations are used. Thus, the compactness and aspect ratio varied from one generation to another in Fig. 10b which led to the observed wall shear stress behavior.

Conclusion

Continuous developments in *lab-on-chip* fabrication have resulted in complex microfluidic networks. Such microfluidic networks are required to operate in an optimum fashion where hydraulic resistance and pressure drop are minimized while wall shear stress is precisely mapped throughout the

network. For instance, in some applications, maintaining the shear stress constant throughout the microfluidic network is required to prevent damage to cells sensitive to shear stress. In other applications such as heavily-laden particulate flow, gradually increasing the shear stress inside the microfluidic network is required to prevent blockage in smaller channels. A combination of theoretical and modeling techniques is used to construct microfluidic networks that achieve the condition of minimum hydraulic resistance and pressure drop while simultaneously maintaining high control over wall shear stress throughout the network. The constraints imposed include constant network volume, constant surface area and constant flow rate. Results obtained from the model are in good agreement with theoretical outcomes. The results show that a global minimum hydraulic resistance is achieved when certain geometric conditions are satisfied. These geometric conditions are related to choosing both the perimeter and area, and thus the compactness and aspect ratio of the parent and daughter branches. The results show that for a rectangular cross-sectional area microfluidic network, the global minimum hydraulic resistance is obtained when the aspect ratio is set to unity, *i.e.* square-cross sectional area. Similarly, the global minimum hydraulic resistance for an isosceles triangular cross-sectional area microfluidic network is achieved when all triangle sides are equal in length (equilateral triangle). This work also demonstrates successful design guidelines for the purpose of controlling the wall shear stress through the bifurcations of the microfluidic network. Increasing, decreasing, and constant wall shear stress throughout a rectangular T-shaped microfluidic network are also presented.

Appendix

Nomenclature

Symbol	Description	Unit
A	Area	m^2
a	Geometric constant	—
b	Geometric constant	—
B	Base length in isosceles triangle	m
C	Compactness ratio	—
d	Depth	m
L	Length	m
l	Leg length in isosceles triangle	m
n	Microchannel generation	—
P	Perimeter	m
p	Pressure	Pa
Q	Volumetric flow rate	$m^3\ s^{-1}$
R	Hydraulic resistance	$kg\ m^{-4}\ s^{-1}$
U	Average velocity	$m\ s^{-1}$
V	Volume	m^3
X	Branching parameter	—
SA	Surface area	m^2
Greek symbols		
μ	Dynamic viscosity	Pa s
β	Geometric factor	—
$\bar{\tau}$	Average wall shear stress	Pa
α_1	Generalized area power coefficient	—
α_2	Generalized perimeter power coefficient	—
ω	Width	m
ε	Aspect ratio	—
Subscript		
in	Inlet	
out	Outlet	
0	Parent channel	
1	Daughter channel	

References

1 D. Huh, *et al.*, Reconstituting organ-level lung functions on a chip, *Science*, 2010, **328**(5986), 1662–1668.
2 D. Huh, *et al.*, Microengineered physiological biomimicry: organs-on-chips, *Lab Chip*, 2012, **12**(12), 2156–2164.
3 J. A. Potkay, *et al.*, Bio-inspired, efficient, artificial lung employing air as the ventilating gas, *Lab Chip*, 2011, **11**(17), 2901–2909.
4 R. W. Barber and D. R. Emerson, Biomimetic design of artificial micro-vasculatures for tissue engineering, *Altern. Lab. Anim.*, 2010, **38**(Suppl 1), 67–79.
5 R. J. Gilbert, *et al.*, Computational and functional evaluation of a microfluidic blood flow device, *ASAIO J.*, 2007, **53**(4), 447–455.
6 R. W. Barber and D. R. Emerson, Optimal design of microfluidic networks using biologically inspired principles, *Microfluid. Nanofluid.*, 2008, **4**(3), 179–191.
7 J. G. Auniņš, *et al.*, Fluid mechanics, cell distribution, and environment in cell cube bioreactors, *Biotechnol. Prog.*, 2003, **19**(1), 2–8.
8 L. Wang, Y. Fan and L. Luo, Lattice Boltzmann method for shape optimization of fluid distributor, *Comput. Fluids*, 2014, **94**, 49–57.
9 J. Berthier, *et al.*, COMSOL assistance for the determination of pressure drops in complex microfluidic channels, in *Comsol Conference*, 2010.
10 J. Wu, D. Day and M. Gu, Shear stress mapping in microfluidic devices by optical tweezers, *Opt. Express*, 2010, **18**(8), 7611–7616.
11 M. Cioffi, *et al.*, A computational and experimental study inside microfluidic systems: the role of shear stress and flow recirculation in cell docking, *Biomed. Microdevices*, 2010, **12**(4), 619–626.
12 C. D. Murray, The physiological principle of minimum work: I. The vascular system and the cost of blood volume, *Proc. Natl. Acad. Sci. U. S. A.*, 1926, **12**(3), 207.
13 K. W. Oh, *et al.*, Design of pressure-driven microfluidic networks using electric circuit analogy, *Lab Chip*, 2012, **12**(3), 515–545.
14 M. S. Razavi, E. Shirani and M. Salimpour, Development of a general method for obtaining the geometry of microfluidic networks, *AIP Adv.*, 2014, **4**(1), 017109.
15 M. Sayed Razavi and E. Shirani, Development of a general method for designing microvascular networks using distribution of wall shear stress, *J. Biomech.*, 2013, **46**(13), 2303–2309.

16 A. L. Marsden, J. A. Feinstein and C. A. Taylor, A computational framework for derivative-free optimization of cardiovascular geometries, *Comput. Methods Appl. Mech. Eng.*, 2008, **197**(21), 1890–1905.
17 P. R. Painter, P. Edén and H.-U. Bengtsson, Pulsatile blood flow, shear force, energy dissipation and Murray's Law, *Theor. Biol. Med. Modell.*, 2006, **3**(1), 31.
18 A. G. Kanaris, A. D. Anastasiou and S. V. Paras, Modeling the effect of blood viscosity on hemodynamic factors in a small bifurcated artery, *Chem. Eng. Sci.*, 2012, **71**, 202–211.
19 A. Anastasiou, A. Spyrogianni and S. Paras, Experimental study of pulsatile blood flow in micro channels, in CHISA, 2010, 19th International Congress of Chemical and Process Engineering, 2010.
20 K. Zografos, *et al.*, *Constant depth microfluidic networks based on a generalised Murray's law for Newtonian and power-law fluids*, 2014.
21 R. Revellin, *et al.*, Extension of Murray's law using a non-Newtonian model of blood flow, *Theor. Biol. Med. Modell.*, 2009, **6**(1), 7–9.
22 Y. Muzychka and J. Edge, Laminar non-Newtonian fluid flow in noncircular ducts and microchannels, *J. Fluids Eng.*, 2008, **130**(11), 111201.
23 A. H. Reis, Laws of non-symmetric optimal flow structures, from the macro to the micro scale, 2012.
24 X. Shan, M. Wang and Z. Guo, Geometry optimization of self-similar transport network, *Math. Probl. Eng.*, 2011, **2011**, 421526.
25 D. M. Hoganson, *et al.*, Principles of biomimetic vascular network design applied to a tissue-engineered liver scaffold, *Tissue Eng., Part A*, 2010, **16**(5), 1469–1477.
26 A. D. Gat, I. Frankel and D. Weihs, Compressible flows through micro-channels with sharp edged turns and bifurcations, *Microfluid. Nanofluid.*, 2010, **8**(5), 619–629.
27 D. Tondeur, Y. Fan and L. Luo, Constructal optimization of arborescent structures with flow singularities, *Chem. Eng. Sci.*, 2009, **64**(18), 3968–3982.
28 O. Tonomura, *et al.*, Optimal Shape Design of Pressure-Driven Microchannels using Adjoint Variable Method. in ASME 2007 5th International Conference on Nanochannels, Microchannels, and Minichannels. 2007. American Society of Mechanical Engineers.
29 N. A. Mortensen, F. Okkels and H. Bruus, Reexamination of Hagen-Poiseuille flow: Shape dependence of the hydraulic resistance in microchannels, *Phys. Rev. E: Stat., Nonlinear, Soft Matter Phys.*, 2005, **71**(5), 057301.
30 D. R. Emerson, *et al.*, Biomimetic design of microfluidic manifolds based on a generalised Murray's law, *Lab Chip*, 2006, **6**(3), 447–454.
31 M. Bahrami, M. Yovanovich and J. Culham, Pressure drop of fully-developed, laminar flow in microchannels of arbitrary cross-section, *J. Fluids Eng.*, 2006, **128**(5), 1036–1044.
32 P. Gadad, *et al.*, Numerical Study of Flow inside the Micro Fluidic Cell Sense Cartridge, *APCBEE Proc.*, 2014, **9**, 59–64.

